Title

Back-end readout electronic design and initial results: a head-and-neck dedicated PET system based on CZT.

Authors

Wang, Yuli

Herbst, Ryan

Abbaszadeh, Shiva

Publication Date

2021-02-01

DOI

10.1117/12.2576598

Peer reviewed

HHS Public Access

Author manuscript

Proc SPIE Int Soc Opt Eng. Author manuscript; available in PMC 2024 November 02.

Published in final edited form as:

Proc SPIE Int Soc Opt Eng. 2021 February ; 11595: . doi:10.1117/12.2576598.

Back-end readout electronic design and initial results: a head-and-neck dedicated PET system based on CZT

Yuli Wang[a], **Ryan Herbst**[b], **Shiva Abbaszadeh**[a]

[a]Department of Electrical and Computer Engineering, University of California, Santa Cruz, Santa Cruz, CA, 95064

[b]SLAC National Accelerator Laboratory, 2575 Sand Hill Road, Menlo Park, CA 94025

Abstract

Cadmium zinc telluride (CZT) radiation detectors are suitable for various applications, due to good energy performance at room temperature and simple pixilation to achieve high spatial resolution. Our group is developing a two-panel head-and-neck dedicated positron emission tomography (PET) system with CZT detectors. In this work, we present the back-end readout electronic design and the initial electronic noise results of our system. The back-end readout electronic incorporates RENA boards (a total 150 RENA boards for each panel), 30:1 fan-in boards connecting 30 RENA boards to the PicoZed 7010/7020 board (a total 5 fan-in boards for each panel). In each panel, 5:1 intermediate boards are used for biasing CZT detectors. The RENA board and the Picozed board are capable of data transmission of 50 Mbps and 6.6 Gbps, respectively. Electronic noise was also quantified using a square wave test pulse that provides charge injection into each channel of the RENA chip in the amount of 75fC/Volt. The pulse amplitude was chosen to generate approximately the same amount of charges as 511 keV photon would provide for each channels. The FWHM electronic noise at 511 keV was measured to be less than 1% (FWHM of 7.80 ± 1.47 ADC units or 4.89 ± 0.92 keV after conversion)

Keywords

Cadmium zinc telluride (CZT); Positron emission tomography (PET); back-end readout electronic; electronic noise; energy resolution

1. INTRODUCTION

The cadmium zinc telluride (CZT) crystals with high stopping power, good energy resolution and high spatial resolution, are commonly used in X-ray and gamma-ray detection. Detection systems with large volume of CZT detectors have been widely used in medical imaging[1, 2] and particle physics.[3–5] We are developing a high-resolution two-panel head-and-neck dedicated positron emission tomography (PET) system with large volume CZT detectors, shown in figure 1.

Send correspondence to S.A.: sabbasza@ucsc.edu.

Compared to the scintillator detector (i.e. lutetium-yttrium oxyorthosilicate (LYSO)[6, 7]), CZT has better performance on the energy resolution and is much easier to achieve high spatial resolution by simple metal electrode deposition.[8] The performance comparison between the LYSO and the CZT detector crystals was conducted in our previous simulation work.[9] We have reported that the two-panel PET system using CZT could achieve higher spatial resolution and achieve higher accuracy in recovering the position of multiple interaction photon events.[10] We have also demonstrated the a two-panel geometry system could improve the spatial resolution of the tumor detection in the small lymph does (< 10 mm).[9] A penalized maximum-likelihood reconstruction algorithms was also been developed in our lab, which could improve limited-angle artifacts in the dedicated head and neck PET system.[11]

In this paper, the CZT detectors we used are with 4.0×4.0×0.5 cm^3 dimensions and are produced by Kromek. The electrode pattern geometry design has been extensively studied and optimized to provide high detector performance. The detail of the CZT detector design and optimization can be found in the references.[12]

In order to maintain the high energy resolution of CZT crystals, in a scaled-up PET system with a large number of CZT detectors (300 CZT crystals), it is crucial to keep the noise of front-end and back-end electronic as low as possible. In addition, high data throughput and effective data transmission is required. In this scenario, there is no commercially available readout electronic system. In this work, we describe the design of the back-end readout electronics and also present the initial electronic noise results of system.

2. MATERIALS AND METHODS

2.1 CZT detector assembly

Each CZT crystal has 39 anode strips, 38 steering electrode strips, and 8 cathode strips as shown in Figure 2 (a) and (b). Two identical CZT crystals shown in Figure 2 (c) are assembled to a common flexible circuit based on anode-cathode-cathode-anode (ACCA) stacking to construct a 4.0×4.0×1.0 cm^3 CZT detector module.

Since the crystals are attached to the flexible circuits, this structure could increase the packing fraction and reduce the dead space between CZT detectors. The cathode and anode bias voltages are −500V and 0V, respectively, while the steering bias voltage is −80V. The final goal is to build a dual-panel head-and-neck PET system with 300 CZT detectors. Each panel comprises a 30-row by 5-column array of CZT detectors stacked on top of each other. The detectors are oriented in an “edge-on” configuration, and thus each incoming photon traverses up to 4 cm of CZT if it is perpendicular to the panel, or slightly more or less if it goes through the panel at an angle.

2.2 Back-end readout electronics

The diagram of back-end readout electronics of one panel is shown in Figure 3. It incorporates RENA boards (a total 150 RENA boards for each panel in a full systems), 30:1 fan-in boards connecting the RENA boards to the PicoZed 7010/7020 board (a total 5 fan-in boards for each panel in full system). In each panel, 5:1 intermediate boards are used

to provide bias high voltage to the CZT detectors. Each CZT module is read out using two RENA-3 ASICs. The RENA-3 board is capable of data transmission at 50 Mbps. PicoZed board has the maximum 6.6 Gbps data transmission capability and is connected to a DAQ computer via fan-in board. Each fan-in board has a PicoZed board with the Xilinix ZYNQ XC7Z030 FPGA and support 30 RENA board.

Figure 4 depicts the final layout of the fan-in board. The fan-in board connects to a 1-column by 30-row array of RENA boards. The 6V DC power and ground from fan-in board are routed individually to each RENA board to avoid crosstalk between boards. In order to avoid logic metastability between subsystems in different clock domains, a single clock domain is enforced across the entire DAQ chain. The fan-in board is responsible for generating the system-wide 50 MHz clock, receiving RENA ASIC timing signal (i.e. UV signal, U and V referred in the data sheet) from a function generator, and distributing the clock and UV signal to all 30 RENA boards attached to it. The fan-in board also provides the Xilinx JTAG chain interface for programming all 30 RENA boards. Lastly, DAQ computer is connected to detector system via fan-in board with the physical connection.

2.3 Measurement of electronic noise of the system

To quantify the contribution of electronic noise of the external circuit on the energy resolution and to estimate a lower bound for energy resolution, first we used a square wave pulse as the excitation source for providing charge injection in each channel. The square wave pulse frequency was 1 kHz with 500 mV peak-to-peak amplitude with no offset, which simulates approximately equivalent charge induced by a 511 keV photon in the CZT crystal. In our preliminary system studies, data were acquired with 18 RENA boards as shown in Figure 5. The spectral peak with full width at half maximum (FWHM) was calculated in both ADC and keV.

3. RESULTS AND CONCLUSION

We summarize the contribution of electronic noise of back-end readout circuit on the energy resolution using test pulse in the table 1. The RENA boards produces a spectral peak with FWHM of 7.80 ± 1.47 ADC units (4.89 ± 0.92 keV after conversion). Our new design head-and-neck system has a better performance when compared the results of previous system with test pulses.[1, 13]

In this paper, we present back-end readout electronic design for head-and-neck dedicated CZT based PET system with low-noise, effective and high-performance. The data acquisition chain of back-end readout electronic, consisting of intermediate board, RENA board, fan-in board (carrying PicoZed 7010/7020) and DAQ computer, are with high data throughput and effective data transmission. This kind of large volume CZT detector system with well designed back-end readout electronic can also be widely used in particle physics, nuclear physics, X-Ray detection and gamma-ray detection.

ACKNOWLEDGMENTS

The authors acknowledge the support from the National Institute of Biomedical Imaging and Bioengineering of the National Institutes of Health under Award Number R01EB028091.

REFERENCES

[1]. Abbaszadeh S, Gu Y, Paul RD, and Levin CS, "Characterization of a sub-assembly of 3d position sensitive cadmium zinc telluride detectors and electronics from a sub-millimeter resolution pet system," Physics in Medicine and Biology 61, 6733 (2016). [PubMed: 27551981]

[2]. Abbaszadeh S and Levin C, "Positioning true coincidences that undergo inter-and intra-crystal scatter for a sub-mm resolution cadmium zinc telluride-based pet system," Physics in medicine and biology 63, p025012 (2018).

[3]. Schlesinger TE, Toney JE, Yoon H, Lee EY, Brunett BA, Franks L, and James RB, "Cadmium zinc telluride and its use as a nuclear radiation detector material," Materials Science and Engineering: R: Reports 32, 4–5 (2001).

[4]. Wang Y, Li Y, Yi F, Li J, Xie S, Peng Q, and Xu J, "Two-crossed-polarizers based optical property modulation method for ionizing radiation detection for positron emission tomography," Physics in Medicine & Biology 64(13), 135017 (2019). [PubMed: 31117057]

[5]. Wang Y, Tao L, Abbaszadeh S, and Levin C, "Further investigations of a radiation detector based on ionization-induced modulation of optical polarization," Physics in Medicine & Biology (2021).

[6]. Li M and Abbaszadeh S, "Depth-of-interaction study of a dual-readout detector based on tofpet2 application-specific integrated circuit," Physics in Medicine & Biology 64(17), 175008 (2019). [PubMed: 31382253]

[7]. Romanchek G, Wang Y, Marupudi H, and Abbaszadeh S, "Performance of optical coupling materials in scintillation detectors post temperature exposure," Sensors 20(21), 6092 (2020). [PubMed: 33120896]

[8]. Li M, Wang Y, and Abbaszadeh S, "Development and initial characterization of a high-resolution pet detector module with doi," Biomedical Physics & Engineering Express 6(6), 065020 (2020). [PubMed: 34234961]

[9]. Li M, Yockey B, and Abbaszadeh S, "Design study of a dedicated head and neck cancer pet system," IEEE transactions on radiation and plasma medical sciences 4(4), 489–497 (2020). [PubMed: 32632397]

[10]. Yang S, Li M, Reed M, Hugg J, Chen H, and Abbaszadeh S, "Effect of czt system characteristics on compton scatter event recovery," IEEE transactions on radiation and plasma medical sciences 4(1), 91–97 (2019). [PubMed: 31922083]

[11]. Zhang H, Wang Y, Qi J, and Abbaszadeh S, "Penalized maximum-likelihood reconstruction for improving limited-angle artifacts in a dedicated head and neck pet system," Physics in Medicine & Biology 65(16), 165016 (2020). [PubMed: 32325441]

[12]. Gu Y, Matteson JL, Skelton RT, Deal AC, Stephan EA, Duttweiler F, Gasaway TM, and Levin CS, "Study of a high-resolution, 3d positioning cadmium zinc telluride detector for pet," 56, 1563 (2011).

[13]. Abbaszadeh S and Levin C, "New-generation small animal positron emission tomography system for molecular imaging," Journal of Medical Imaging 4, p011008 (2017).

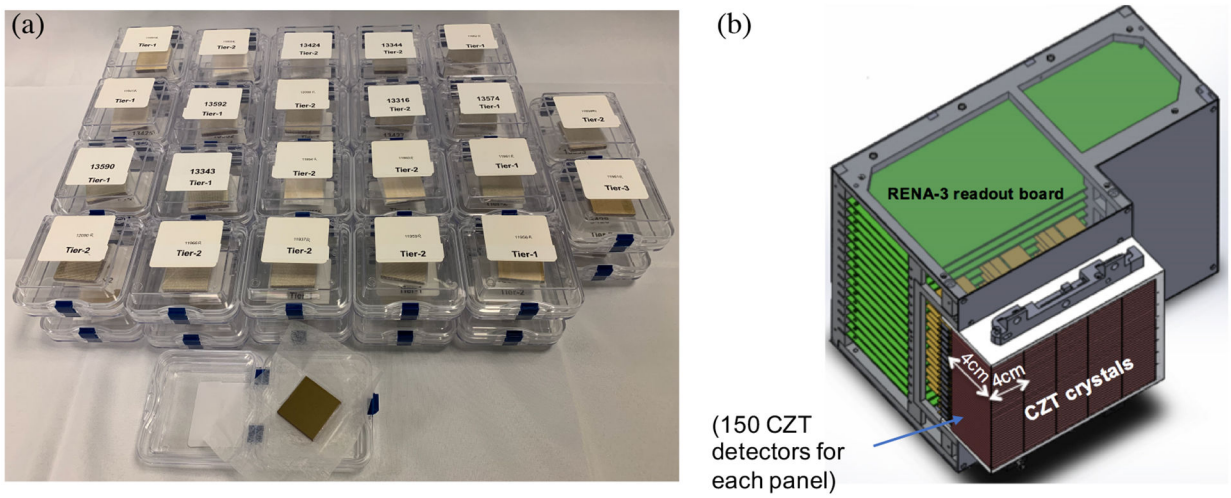

Figure 1.

(a) Diagram of 45 CZT crystal detectors, (b) Schematic of CZT based PET system with 30-row by 5-column of CZT detectors.

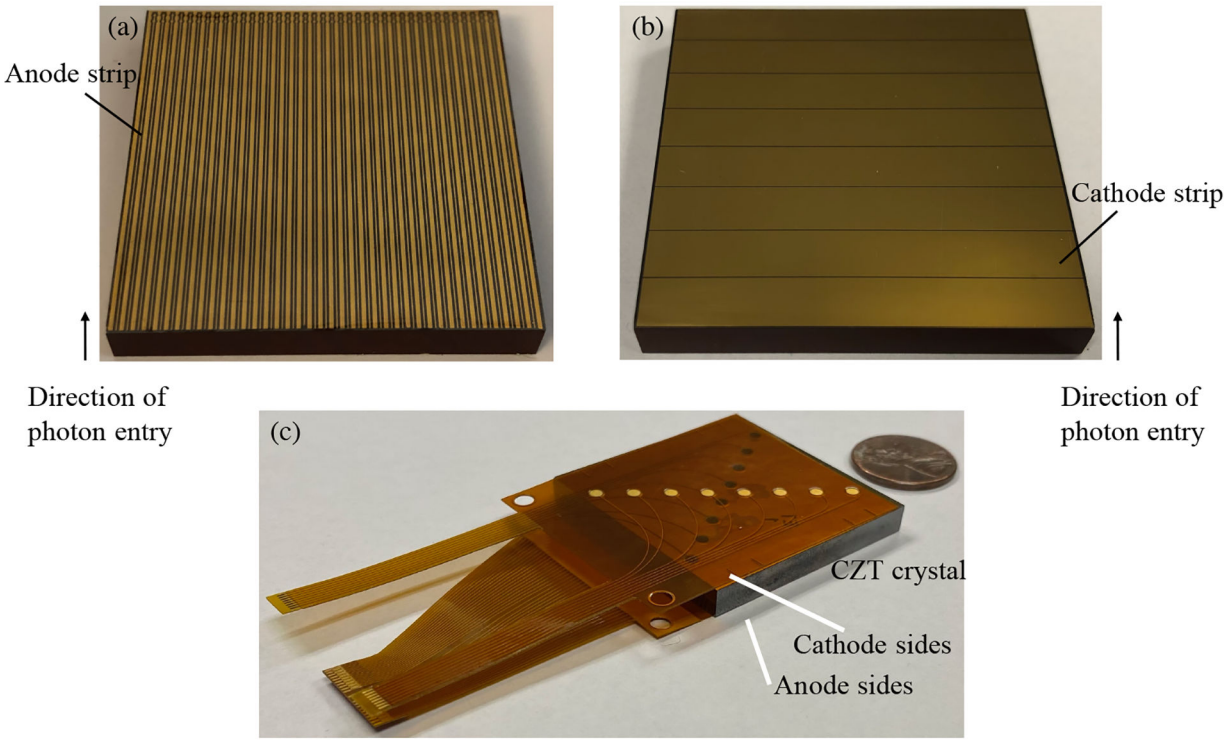

Figure 2.
Schematic of CZT crystal with (a) anode electrode pattern and (b) cathode electrode pattern, (c) 4.0×4.0×0.5 cm^3 CZT crystal assembled with flexible circuit.

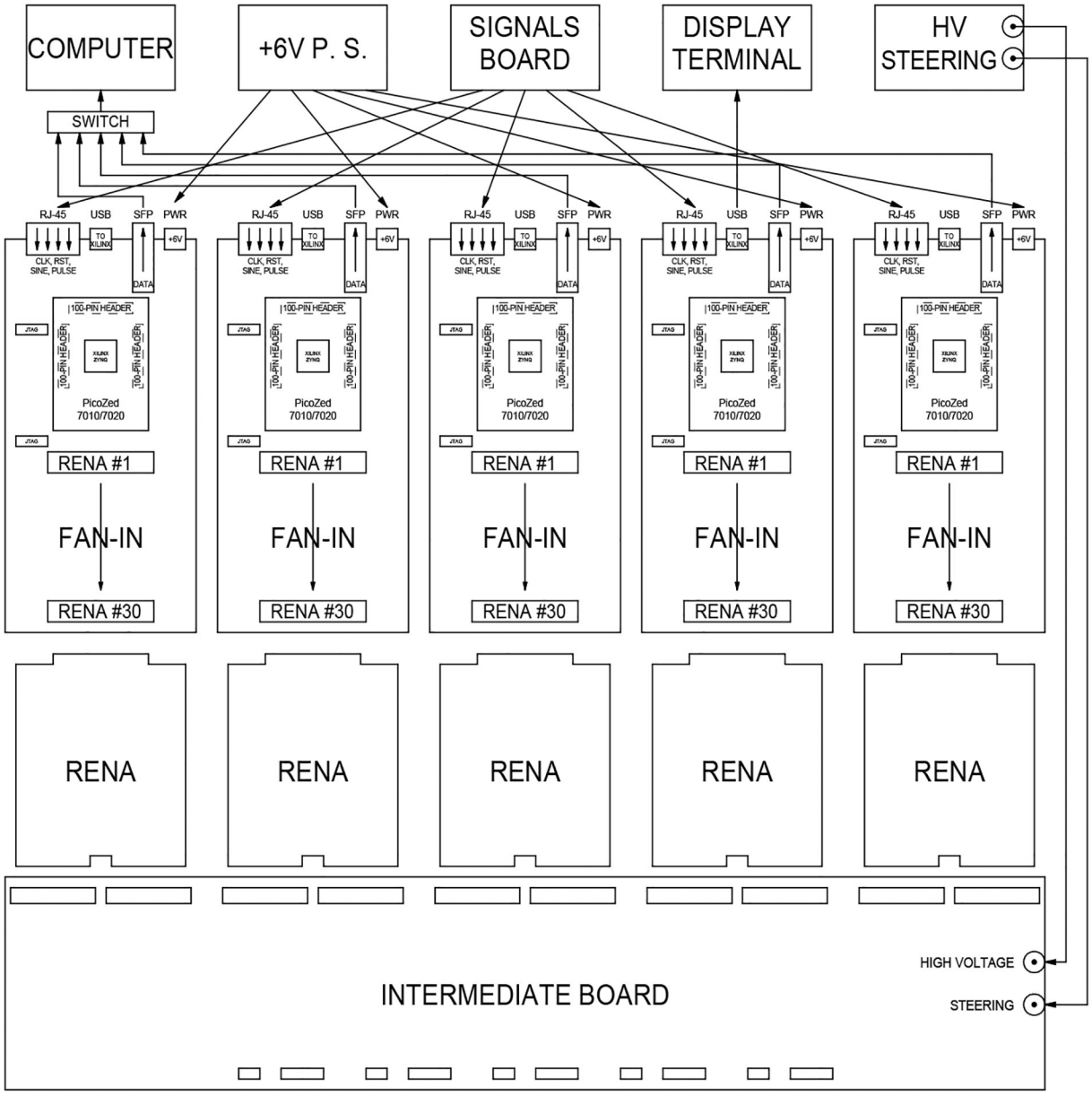

Figure 3.
The schematic of back-end readout electronic of one panel.

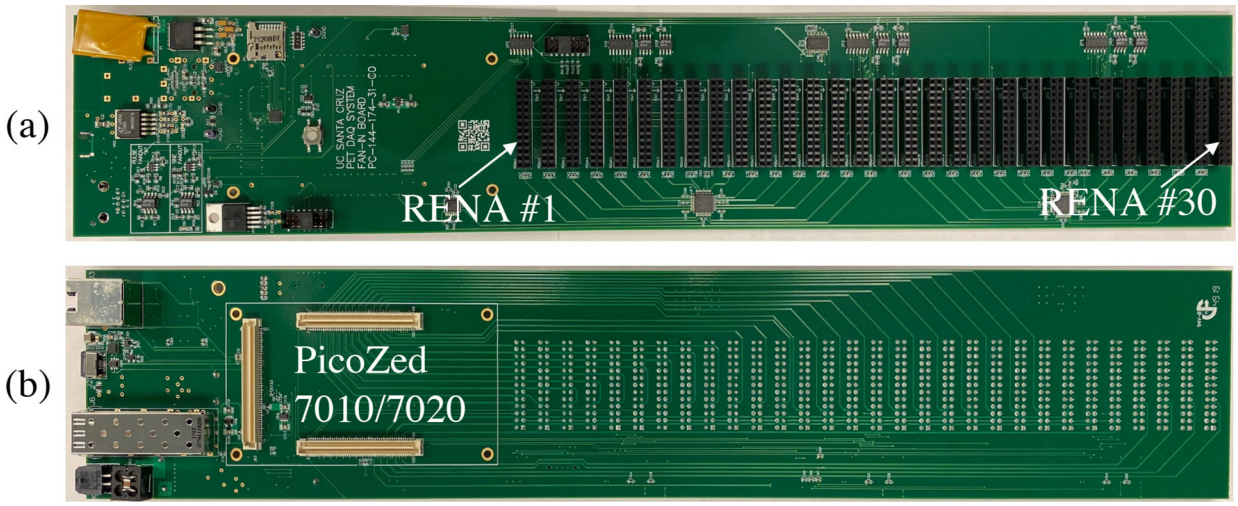

Figure 4.
Layout of the fan-in board, which measures 8.10cm × 43.3cm.

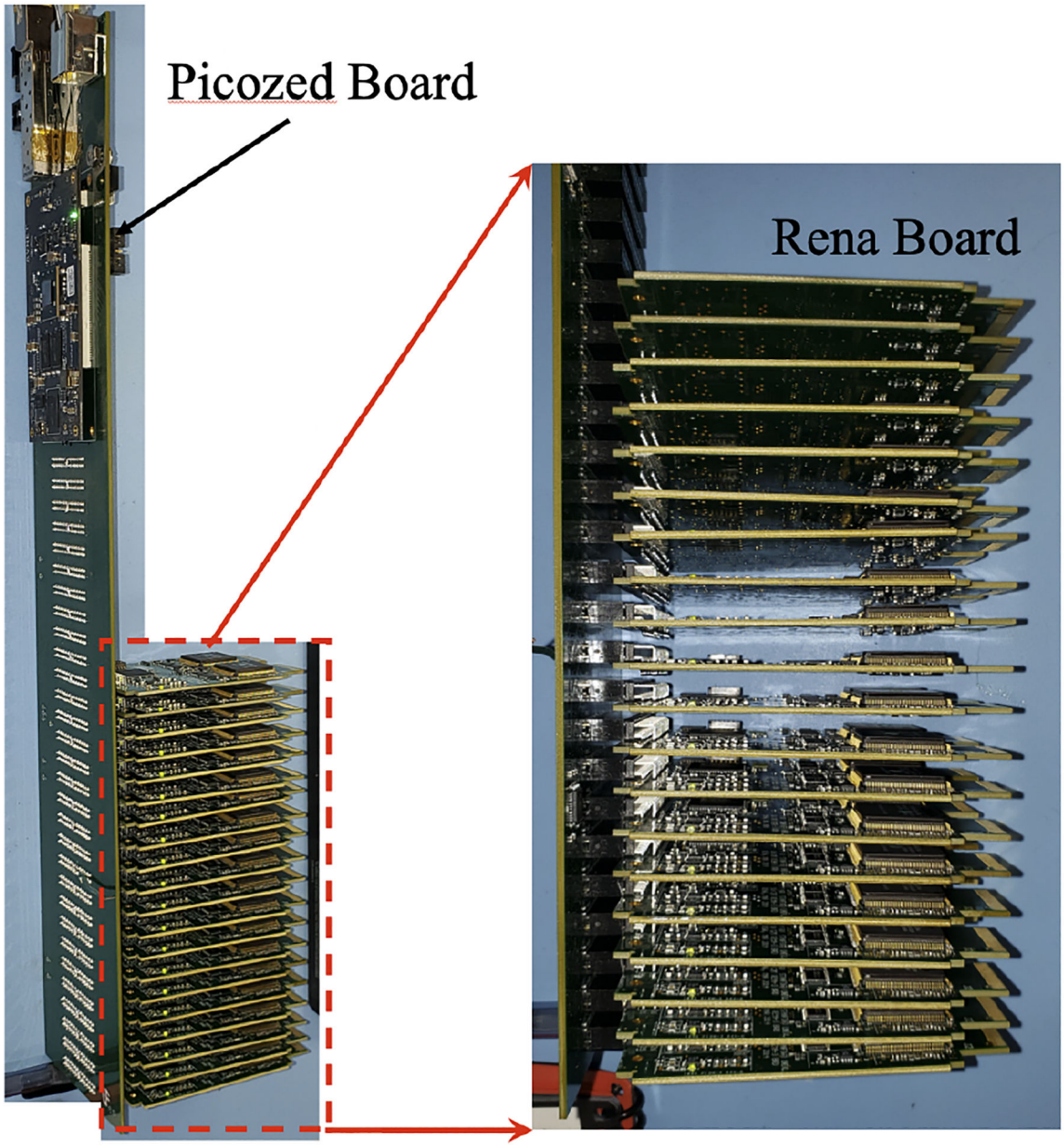

Figure 5.
Diagram of fan-in board assembled with RENA boards.

Table 1.

FWHM energy resolution with 18 RENA boards using test pulse

Circuit condition	Noise source	FWHM of keV units	FWHM energy resolution (%)
RENA board only	Best case	4.89 ± 0.92	0.96 ± 0.18